Author Manuscript

Author Manuscript

Author Manuscript

Author Manuscript

HHS Public Access

Author manuscript

Biochim Biophys Acta Gen Subj. Author manuscript; available in PMC 2021 January 01.

Published in final edited form as:

Biochim Biophys Acta Gen Subj. 2020 January ; 1864(1): 129455. doi:10.1016/j.bbagen.2019.129455.

Characterization of 5'-Methylthioadenosine/S-Adenosylhomocysteine Nucleosidases from *Borrelia burgdorferi*: Antibiotic Targets for Lyme Disease

Kenneth A. Cornell[a,b,#], **Reece J. Knippel**[a], **Gerald R. Cortright**[a], **Meghan Fonken**[a], **Christian Guerrero**[a], **Amy R. Hall**[a], **Kristen A. Mitchell**[b,c], **John H. Thurston**[d], **Patrick Erstad**[d,e], **Aoxiang Tao**[e], **Dong Xu**[e], **Nikhat Parveen**[f]

[a]Department of Chemistry & Biochemistry, Boise State University, Boise, Idaho, USA

[b]Biomolecular Research Center, Boise State University, Boise, Idaho, USA

[c]Department of Biological Sciences, Boise State University, Boise, Idaho, USA

[d]Department of Chemistry, The College of Idaho, Caldwell, Idaho, USA

[e]Department of Biomedical & Pharmaceutical Sciences, Idaho State University, Meridian, Idaho, USA

[f]Department of Microbiology, Biochemistry and Molecular Genetics, Rutgers New Jersey Medical School, Newark, New Jersey, USA

Abstract

Background.—*Borrelia burgdorferi* causes Lyme disease, the most common tick-borne illness in the United States. The Center for Disease Control and Prevention estimates that the occurrence of Lyme disease in the U.S. has now reached approximately 300,000 cases annually. Early stage *Borrelia burgdorferi* infections are generally treatable with oral antibiotics, but late stage disease is more difficult to treat and more likely to lead to post-treatment Lyme disease syndrome.

Methods.—Here we examine three unique 5'-methylthioadenosine/S-adenosylhomocysteine (MTA/SAH) nucleosidases (MTNs or MTANs, EC 3.2.2.9) responsible for salvage of adenine and methionine in *B. burgdorferi* and explore their potential as antibiotic targets to treat Lyme disease. Recombinant *Borrelia* MTNs were expressed and purified from *E. coli*. The enzymes were extensively characterized for activity, specificity, and inhibition using a UV spectrophotometric assay. *In vitro* antibiotic activities of MTN inhibitors were assessed using a bioluminescent BacTiter-Glo™ assay.

Results.—The three *Borrelia* MTNs showed unique activities against the native substrates MTA, SAH, and 5'-deoxyadenosine. Analysis of substrate analogs revealed that specific activity rapidly dropped as the length of the 5'-alkylthio substitution increased. Non-hydrolysable nucleoside

[#]Address correspondence to Kenneth A. Cornell, kencornell@boisestate.edu.

Publisher's Disclaimer: Disclaimer. The funding agencies had no role in study design, data collection and interpretation, or the decision to submit the work for publication. The contents of this manuscript are solely the responsibility of the authors and do not represent the official views of NIH, NSF, or other funding agencies. The authors declare no competing financial interests or other conflicts of interest in the submission and publication of this manuscript.

Author Manuscript Author Manuscript Author Manuscript Author Manuscript

transition state analogs demonstrated sub-nanomolar enzyme inhibition constants. Lastly, two late stage transition state analogs exerted *in vitro* IC_{50} values of 0.3–0.4 μg/mL against cultured *B. burgdorferi* cells.

Conclusion.—*B. burgdorferi* is unusual in that it expresses three distinct MTNs (cytoplasmic, membrane bound, and secreted) that are effectively inactivated by nucleoside analogs.

General Significance.—The *Borrelia* MTNs appear to be promising targets for developing new antibiotics to treat Lyme disease.

Keywords

Borrelia; MTA/SAH Nucleosidases; MTAN; MTN; transition state analog; Lyme disease

1. Introduction

According to the CDC, *Borrelia burgdorferi* causes approximately 300,000 cases of Lyme disease in the U.S. each year.[1,2] The Lyme spirochaetes are transmitted by ticks of the genus *Ixodes* that commonly feed on the white-footed mouse and other small mammals, with deer being the preferred host for adult female ticks. Lyme disease is most commonly reported in the northeast and Great Lakes states, but infected ticks have increasingly been found in western and southern states, which means that much of the U.S. population is at risk of contracting the disease.[3]

Lyme disease is diagnosed based on symptoms such as fever, fatigue, and a characteristic bull's-eye rash (erythema migrans) at the site of the tick bite. Early stage disease is generally treatable with a 2 to 3-week course of oral doxycycline, cefuroxime axetil, or amoxicillin antibiotics. For patients who are intolerant of these drugs, macrolides may be used, but they are found to be less effective.[4,5] Lack of prompt treatment or treatment failure can lead to disease progression and increased severity of symptoms, such as arthritis or joint swelling, headaches, facial palsy, and peripheral neuropathies. In these cases, antibiotic treatment is less successful and there is increasing likelihood of the development of post-treatment Lyme disease syndrome that may take months or even years to resolve.[6–11]

In recognition of the increasing prevalence of Lyme disease, the relatively small arsenal of antibiotics available to treat *Borrelia* infections, and the eventual likelihood of widespread antibiotic resistance, we have begun to explore the development of novel antibiotics that target unique nucleosidases (MTNs) found in the *Borrelia* spirochaete. *B. burgdorferi* is unique in that it possesses three MTNs.[12] The first enzyme, Bgp (*Borrelia* glycosaminoglycan-binding protein), is a membrane-bound or secreted enzyme encoded by the *bb0588* gene.[13–17] This protein functions both as an adhesin facilitating adherence to the host cells through ubiquitously present glycosaminoglycans, and as an MTN. The second enzyme, Pfs, is a cytoplasmic homolog of the *E. coli* Pfs enzyme. We have previously showed that both Bgp and Pfs exhibit nucleosidase activities and performed initial studies of enzyme specificity.[16,18,19] Borrelial Pfs is encoded by the *bb0375* gene as part of an operon that includes the genes for S-adenosylmethionine (SAM, AdoMet) synthetase (MetK) and ribosylhomocysteinase (LuxS) proteins,[20] which are also involved in SAM metabolism (Fig.

Author Manuscript Author Manuscript Author Manuscript Author Manuscript

1). The third enzyme, which is encoded by the endogenous plasmid-borne *bbi06* gene, is designated MtnN. While MtnN has not been previously characterized, it contains a leader sequence that suggests it is secreted and thus has a role in extracellular nucleoside catabolism. All three MTNs are responsible for the catabolism of the three native nucleosides: MTA, SAH, and 5'dADO, which are byproducts of SAM-dependent polyamine synthesis, methylations, and radical SAM reactions, respectively (Fig. 1).[21] In the context of the underlying purine auxotrophy of *Borrelia* species,[22] and 70% A-T rich genome, these MTNs probably play a critical role in the salvage of nutritionally valuable adenine from intracellular and extracellular nucleoside sources. Our prior work showed that several nucleoside analogs were inhibitors of Bgp and Pfs activity and produced *in vitro* anti-borrelial effects.[19] It is difficult to assess if one or more of these MTNs are essential for *B. burgdorferi* survival due to difficulty in generating multi-gene mutants in this spirochaete. Although mutants lacking Bgp are not defective in growth in the rich BSKII culture medium that contains 6% rabbit serum, they are significantly attenuated in causing infection and disease in the nutritionally limited environment of the host[16,23]. In the work presented here, we extensively characterize the three borrelial MTNs for substrate specificity and kinetics and report on the enzyme inhibitory effects of a panel of transition state analogs, and their antibiotic effects against *B. burgdorferi* cultures. The results support the continued development of MTN inhibitors as a new class of antibiotics to treat Lyme disease.

2. Materials & Methods

2.1. Chemicals, media, substrates, and inhibitors.

Buffer constituents, Luria-Bertani (LB) media, restriction endonucleases and antibiotics (ampicillin, kanamycin) were purchased from ThermoFisher Scientific (Pittsburgh, PA). BSK-II media containing 6% rabbit serum, the substrates (MTA, SAH, 5'dADO), nucleosides (adenosine, 5'-chloroadenosine) and nucleotide (5'-adenosine monophosphate) were obtained from Sigma-Aldrich (St. Louis, MO). Nucleoside analogs (5'-ethylthioadenosine [ETA], 5'-propylthioadenosine [PTA], 5'-isopropylthioadenosine [iPTA], 5'-butylthioadenosine [BTA]) were the kind gift of Dr. Michael Riscoe (Portland VA Medical Center, Portland, OR). The early stage transition state analogs, 1-(9-deazaadenin-9-yl)-1,4-dideoxy-1,4-imino-5-methylthio-D-ribitol (MT-ImmA), 1-(9-deazaadenin-9-yl)-1,4-dideoxy-1,4-imino-5-homocysteinyl-D-ribitol (HCY-ImmA), 1-(9-deazaadenin-9-yl)-1,4-dideoxy-1,4-imino-5-deoxyethyl-D-ribitol (5'-dEt-ImmA) were the kind gift of Dr. YS Babu (BioCryst Pharmaceuticals, Birmingham, AL). The late stage transition state analogs, 1-[(9-deazaadenin-9-yl) methyl]-3-hydroxy-4-(methylthiomethyl) pyrrolidine (MT-DADMe-ImmA), and 1-[(9-deazaadenin-9-yl)methyl]-3-hydroxy-4-(butylthiomethyl)pyrrolidine (BuT-DADMe-ImmA) were graciously provided by Dr. Vern Schramm (Albert Einstein College of Medicine, Bronx, NY).

2.2. MTN gene cloning and sequence analysis.

We have previously reported on the construction of expression plasmids for recombinant *Borrelia* Bgp and cytoplasmic Pfs enzymes.[16,19] The *B. burgdorferi mtnN* (*bbi06*) gene was PCR-amplified using high fidelity *herculase* enzyme (Agilent Technologies, Santa Clara, CA) and genomic DNA template from the infectious N40 strain. Gene specific forward

Author Manuscript Author Manuscript Author Manuscript Author Manuscript

(5'IntBB106Bam CGGGATCCAATATTTTAATAATCTCAGCTACA) and reverse (3'BBI06Pst AACTGCAGTTACATTAACTTAATTAAGTTTTCTA) primers were used to amplify a truncated BBI06 gene that lacked the signal peptide but contained introduced BamHI and PstI restriction endonuclease sites (underlined). PCR temperature cycling conditions consisted of 95°C (2 min), followed by 35 cycles of 95°C (1 min), 48°C (30 sec), and 65°C (1 min). After cloning the PCR product in Topo-XL vector (Invitrogen, Carlsbad, CA), the insert was released using BamHI and XhoI for subsequent cloning into the pET30a plasmid vector (Merck, Darmstadt, Germany), and sequenced to confirm the fidelity of the *mtnN* gene and in-frame fusion with the 5'-hexahistidine coding region. The plasmid was transformed into chemically competent *E. coli* BL21(DE3)pLysS cells according to the manufacturer's protocol (Invitrogen, Carlsbad, CA) and transformants selected on LB agar supplemented with 50 μg/mL kanamycin. Amino acid sequence alignments between the *E. coli* MTN and *B. burgdorferi* Bgp, MtnN, Pfs enzymes were performed using the Clustal Omega multiple sequence alignment tool[24] accessed through the ExPASy bioinformatics resource portal (https://www.expasy.org/resources).

2.3. Expression and purification of recombinant MTNs.

Overnight 10 mL cultures of recombinant *E. coli* BL21(DE3)pLysS cells containing engineered pET30a expression plasmids for Bgp, MtnN or Pfs were grown at 37°C with shaking (225 rpm) in LB broth supplemented with 50 μg/mL kanamycin and 0.5% glucose ($LB_{kan}{}^{50}{}_{glucose}{}^{0.5\%}$). The culture was diluted 1:50 in fresh $LB_{kan}{}^{50}{}_{glucose}{}^{0.5\%}$ and incubated at 37°C with shaking (225 rpm) until the absorbance (600 nm) reached 0.4–0.6. Protein expression was induced with the addition of isopropyl β-D-1-thiogalactopyranoside (IPTG) to a final concentration of 1 mM and continued overnight incubation with shaking at 30°C. Cells were harvested by centrifugation (10,000×g/15 min), and the pellet was washed once with ice-cold lysis buffer (50 mM sodium phosphate, pH 8.0, 300 mM NaCl, 10 mM imidazole, 2 mM β mercaptoethanol). Harvested cell pellets were resuspended in 10 mL fresh lysis buffer and lysed by sonication on ice using a Misonix Sonicator 300 (power setting 7, pulse 30 sec, 1 min cooling, 2.5 min total sonication). The cell lysates were centrifuged at 10,000×g for 15 min at 4°C to remove debris, and the lysate was further filtered through a 0.45 μm syringe filter to obtain a clear extract.

N-terminal polyhistidine-tagged MTN proteins were purified from the filtered lysates using cobalt-affinity chromatography according to manufacturer's instructions (ThermoFisher Scientific). Briefly, clarified cell lysates were mixed with 1 mL HisPur™ Cobalt resin overnight at 4°C. The mixture was then transferred to a small column, washed sequentially with ice-cold lysis buffer (pH 8.0) and ice-cold lysis buffer supplemented with 50 mM imidazole. The recombinant MTNs were specifically eluted with lysis buffer supplemented with 250 mM imidazole. Elution fractions containing protein were identified using BioRad Protein Assay reagent (BioRad, Hercules, CA) according to the manufacturer's microassay procedure for microtiter plates. Fractions containing protein concentrations greater than 0.5 mg/mL were pooled, and the final protein concentrations were assessed using scanning UV/vis spectroscopy and Beer's law ($A = \varepsilon lC$). The extinction coefficients used to calculate 1 mg/mL enzyme concentrations from A_{280} absorbance were 0.594 (Bgp), 0.637 (MtnN),

Author Manuscript Author Manuscript Author Manuscript Author Manuscript

0.404 (Pfs), and were based on ExPASy ProtParam computational estimates[25] that were confirmed experimentally.

2.4. Enzyme activity and kinetics.

MTN activity was determined using a spectrophotometric assay that measures the drop in absorbance at 275 nm that occurs when the nucleoside substrate is converted to adenine and the corresponding sugar.[26] Enzyme reactions were performed in UV clear cuvettes using a Cary100 spectrophotometer outfitted with WinUV software (Agilent, Santa Clara, CA). To determine the optimal pH for each enzyme, reaction conditions contained 100 μM MTA, and 100 mM buffer: sodium phosphate-citric acid (pH 4–6), sodium phosphate (pH 6–8) or tris (8.5–8.8). Specific activities for each of the native nucleoside substrates (MTA, SAH, 5'dADO) and nucleoside analogs (ETA, PTA, iPTA, BTA, ADO, ClADO, AMP) contained 100 μM substrate and 100 mM sodium phosphate-citric acid or sodium phosphate buffer at the optimal pH for each enzyme (Pfs, pH 5; Bgp and MtnN, pH 7) in a final reaction volume of 1 mL. Reactions were initiated with the addition of 1–4 μg enzyme, and the velocity of the reaction calculated using a Δε for conversion of nucleoside to adenine of 1600 $M^{-1}cm^{-1}$.[26] Velocity values were converted to units (U) per mg enzyme, where 1U = 1 μmol nucleoside converted per minute. Kinetic constants for all three of the MTNs for each of the native substrates (MTA, SAH, 5'dADO) were determined at the optimal pH for activity and varying the concentration of substrate from 1–100 μM (specifically, 1, 2, 3.3, 4, 5, 6.7, 10, 100 μM) in the enzyme assays, with every concentration tested at least in triplicate. Data on substrate-velocity plots (not shown) were fit to the Michaelis-Menton equation $\left(V_o = \frac{V_{max}[s]}{K_m + [s]}\right)$ using GraphPad Prism version 6.0 software (GraphPad, La Jolla, CA). All kinetic constants were determined from at least three independent experiments.

2.5. MTN inhibitor analysis.

Inhibition constants were determined using the UV assay described above. Reactions with 100 μM MTA substrate and 50–1000 nM transition state analog were initiated by the addition of 0.5 μg enzyme (~18 nM) in a final volume of 1 mL. Reactions were allowed to proceed for 60 min at 22°C. Control reactions contained either no inhibitor or no enzyme. To determine the early onset inhibition constant (K_i), the ratio of the initial inhibited velocity (V_o') vs. uninhibited velocity (V_o) was plotted as a function of inhibitor concentration [I], and the data were fit to the equation for competitive inhibition: $\left(\frac{V'_o}{V_o} = \frac{K_m + [s]}{K_m + [s] + K_m[I]/K_i}\right)$ using GraphPad Prism software. For concentrations of inhibitor that were < 10 fold greater than the enzyme concentration, the effective inhibitor concentration was calculated according to Singh et al.[26] using the equation: $I' = I - \left(1 - \frac{V'_o}{V_o}\right)Et$. The transition state analogs all displayed a second linear reaction rate consistent with previous reports of their actions as slow-onset inhibitors of the *E. coli* and *Streptococcus* MTNs.[26,27] The second linear velocity (V_o*) was measured between 20 and 40 min of the reaction, and the V_o*/V_o ratio was plotted against inhibitor concentration. To determine the slow-onset inhibition

Author Manuscript Author Manuscript Author Manuscript Author Manuscript

constant (K_i*), the data were fit to the equation for competitive inhibition, replacing K_i with K_i* in the equation.

2.6. Homology modeling and molecular docking.

The crystal structure of *Borrelia burgdorferi* Pfs (GI: 488620239) was obtained from Protein Data Bank (PDB ID: 4L0M).[28] Homology modeling of Bgp (GI: 488733690) and MtnN (GI: 11496743) was carried out using Maestro and Prime (version 4.2) of Schrödinger Drug Discovery Suite.[29,30] Sequence alignment of Bgp and MtnN with the non-redundant PDB database was conducted using a BLAST search[31] and the structure prediction wizard in Prime.[30] Template protein structures were selected based on their sequence homology to the query sequences, alignment scores, and gaps between the query and template. The three-dimensional Bgp structure was modeled using the *Borrelia burgdorferi* MTN crystal structure (PDB ID: 4L0M) as the template. The MtnN structure was modeled using the *Vibrio cholera* MTN crystal structure (PDB ID: 4×24) as the template. Both templates provided the best coverage and sequence identity compared to the query sequences near the active site region, respectively. Using the energy-based homology modeling approach in Prime, Bgp and MtnN homology models were constructed as homodimers and superimposed with the Pfs structure (PDB ID: 4L0M) using Maestro. Adenine was then added to the active sites of the Bgp and MtnN homology models from the superimposed Pfs structure. Side chain refinement was performed at the active site and surrounding residues to further optimize the homology models.

Ligand docking was performed using Glide (version 6.9) in Schrödinger.[32,33] Docking grids were generated using default parameters on each of the MTN structures, with the grids centered in the active site and a search radius of 17 Å. Molecular docking was performed using the standard precision (SP) mode and default parameters in Glide. Results were visualized in Maestro and images were rendered using PyMOL (version 1.8).[34]

2.7. Cytotoxicity studies.

The *B. burgdorferi* infectious N40 strain was cultured at 33°C in BSKII media containing 6% rabbit serum (BSK-H) to a density of 10^8 spirochaetes/mL. Cell density was confirmed using a LIVE/DEAD® Fixable Dead Cell Stain Kit (Molecular Probes, Eugene, OR) with subsequent visualization on a hemocytometer under 400× magnification using an EVOS fluorescence microscope. Drug cytotoxicity studies were conducted in 96-well black, clear-bottom plates containing 90 μL spirochaete culture (4×10^6 cells) and 10 μL drug dilution (0.02–10.0 μg/mL final concentration) in BSK-H medium. All drug concentrations were tested in quadruplicate, and each experiment was repeated twice. Wells containing untreated cells served as the 100% positive growth control. Negative controls consisted of wells containing cells treated with 0.2% sodium azide. Plates were sealed with sterile tape and incubated at 33°C in a 5% CO_2/95% humidified air incubator. After 24 hr, antibiotic effects were measured using a previously reported bioluminescence assay for cell viability.[35] In brief, 100 μL of BacTiter-Glo™ reagent (Promega Corporation, Madison, WI) was added to each well, and the luciferase-mediated bioluminescence was measured on a BioTek SynergyHT plate reader. The mean percentage of viable cells was determined using untreated cells as the 100% maximal growth control. The drug concentration required to

Author Manuscript Author Manuscript Author Manuscript Author Manuscript

inhibit 50% of the viability (IC_{50}) was determined using a non-linear fit of the data in GraphPad Prism software.

3. Results & Discussion

3.1. MTN sequence analysis.

The importance of MTN activity for *B. burgdorferi* metabolism is underscored by the fact that its genome encodes three unique MTNs: a cytoplasmic Pfs, and the larger membrane bound and/or secreted Bgp and MtnN enzymes. This abundance of MTN orthologs may represent an adaptation to overcome purine auxotrophy and enhance the salvage of adenine from both cytoplasmic and extracellular host-derived MTA, SAH, and 5'dADO nucleoside pools. A Clustal Omega alignment to the reference cytoplasmic *E. coli* MTN (Fig. 2) shows modest homology to borrelial Bgp (34%), MtnN (28%), and Pfs (38%). However, the percent identity is much higher within borrelial enzyme sequences, with the cytoplasmic Pfs showing 49% and 51% identity to Bgp and MtnN, respectively. Importantly, the three active site aspartate and glutamate residues that are essential for catalysis[36] are completely conserved between all of the enzyme orthologs (indicated in bold underlined type in Fig. 2).

It is also notable that both Bgp and MtnN have amino terminal signal peptide sequences characteristic of membrane bound or secreted proteins (underlined, Fig. 2). Bgp is a glycosaminoglycan binding protein that has been reported to be localized to the borrelial outer cell membrane[16] and secreted into the extracellular environment,[13] which indicates that the signal peptide cleavage site is functional. This was also confirmed by amino-terminal sequence analysis from protein purified from *B. burgdorferi*.[16] Less is known about the plasmid encoded MtnN, but the presence of a N-terminal leader sequence is consistent with an exported enzyme that would function as a surface, periplasmic, or extracellular nucleosidase to supply soluble adenine for uptake by the spirochaete.

3.2. MTN enzyme activity and kinetics.

To explore the potential for *Borrelia* MTNs to serve as antibiotic targets, the corresponding genes were expressed as hexahistidine-tagged proteins and their enzymatic activity extensively characterized. Based on SDS-PAGE analysis, the molecular weights of the purified recombinant monomeric enzymes were determined to be 28–32 kD (Fig. 3), which is consistent with the predicted mass of these MTNs, based on the exclusion of the signal sequence and fusion to the N-terminal purification sequence encoded on the pET30a vector. All of the nucleosidases exhibited enzymatic activity against MTA, but optimal activity varied according to pH. The cytoplasmic Pfs showed a preference for acidic conditions, with the optimal activity seen at pH 5 (Fig. 4). In contrast, the membrane bound/secreted Bgp and MtnN enzymes displayed peak activity at a neutral pH, which is consistent with the pH of the blood and synovial fluid environments (pH 7.4), in which these enzymes would be exposed to in the human host.

All three enzymes carried out hydrolysis of MTA, SAH, and 5'dADO, but each exhibited distinct kinetic parameters for these native substrates (Table 1). Pfs showed the highest catalytic rate constants for the three substrates (k_{cat} = 94–162 min^{-1}) and, uniformly, the

Author Manuscript Author Manuscript Author Manuscript Author Manuscript

highest catalytic efficiencies (118–175 $min^{-1}\mu M^{-1}$). Of the three enzymes, Bgp showed the most selectivity for MTA with an efficiency of 228 $min^{-1}\mu M^{-1}$, which is approximately 4-fold higher than its efficiency for either SAH or 5'dADO (51–53 $min^{-1}\mu M^{-1}$). We have previously reported on Bgp and Pfs preliminary specific activity and Michaelis constants for the substrates MTA and SAH that are consistent with our results reported here.[16,19] However, this is the first report of MtnN nucleosidase activity against any substrate, and the most extensive characterization of substrate specificity for all three of the enzymes against both native nucleosides (MTA, SAH, 5'dADO) that are the products of cellular metabolic reactions, non-subtrate nucleosides/nucleotides (ADO, AMP), and artificial or non-native nucleoside analogs with 5'-alkylthio substitutions (Table 2). In addition, this is the first demonstration of *Borrelia* nucleosidase activity against 5'-deoxyadenosine, and the first report of catalytic rate constants (k_{cat}) and catalytic efficiency (k_{cat}/Km) for the three nucleoside substrates for all three enzymes. Compared to Pfs and Bgp, MtnN showed the lowest activity against the three nucleoside substrates (efficiencies of 4–16 $min^{-1}\mu M^{-1}$), and appeared to prefer SAH as a substrate. The reduced activity of MtnN against the other two nucleosides can largely be attributed to the higher Michaelis constants for MTA (K_m = 9.1 μM) and 5'dADO (K_m = 10.5 μM), as well as somewhat lower catalytic rates (k_{cat} = 33–93 min^{-1}) shown by MtnN against all three nucleosides.

The enzyme-specific activities for each of the three substrates (MTA, SAH, 5'dADO) and a series of 5'-substituted nucleoside analogs were examined to further characterize the active site for drug development efforts. The three enzymes showed specific activities of 4.2–6.89 U/mg for these substrates (Table 2), and MTA was identified generally as the best native substrate for all three enzymes. For neutral 5'-alkylthio substituted nucleoside analogs (ETA, PTA, iPTA, BTA), the enzyme specific activities were reduced by 67–88% as the carbon length of the substitution increased. Of the three enzymes, the specific activity of enzymes for substrates with longer 5'-carbon chain substitutions, such as BTA, was low (12–33% of MTA activity). Replacing the hydrophobic 5'-alkylthio groups with the more electronegative moieties found in adenosine, 5'-chloroadenosine (ClADO), or adenosine monophosphate (AMP) resulted in dramatic losses in activity. The percent of maximum specific activity for adenosine (5–26% of MTA) and AMP (1–3% of MTA) indicate that these other nucleosides/nucleotides are probably not significant substrates for the enzymes under native conditions. These results likely reflect the non-favorable thermodynamic interactions between the electronegative hydroxyl-, phosphoryl-, chloro- groups and the hydrophobic 5'-alkylthio binding pocket. The electronegative nature of these substitutions may also decrease the formation of the ribooxocarbenium ion reaction intermediate, thus reducing the ability of C1 of the sugar to serve as a target for a nucleophilic water molecule.[26]

3.3. MTN inhibitor analysis.

Transition state analogs have been extensively studied as MTN inhibitors.[26,27,37–47] The structures of these inhibitors are based on the ribooxocarbenium ion character of the catalytic intermediate that occurs as the nucleoside substrate is converted to the adenine and sugar products.[26] A primary feature of early transition state structure is protonation of N7 of the adenine ring, which is seen in all of the immucillin analogs (Table 3). Additional features include replacement of the ring oxygen with a nitrogen to mimic the carbocation reaction

Author Manuscript Author Manuscript Author Manuscript Author Manuscript

intermediate and replacement of N9 of the purine ring with a carbon to create a non-hydrolysable glycosidic linkage. Late stage transition state analogs are similar, but the ring nitrogen is moved to the 1'-position, the 2'-hydroxyl group is absent, and a methylene group is added between the ribitol and purine ring to mimic the separate adenine and sugar products of the MTN reaction.

In our studies, transition state analogs were examined for enzyme inhibitory activity using a spectrophotometric assay that measures the decrease in absorbance at 275nm that accompanies the conversion of MTA to adenine and MTR (Fig. 5, top panel). Increasing the concentration of inhibitor (MT-DADMe-ImmA, inset) resulted in a decrease in the slope of the absorbance change, and thus a decrease in the enzyme velocity. Initial inhibition constants were calculated from enzymatic velocities determined in the first 5 minutes of the experiment. As the experiment progressed, distinct changes to the enzyme velocity resulted in a second linear slope between 20–40 min, which is consistent with prior work on the MTNs found in *E. coli* and other bacteria,[26,27] demonstrating that these transition state analogs show slow-onset inhibition. To calculate initial inhibition constants, the ratio of the initial inhibited velocity to uninhibited velocity (V_o'/V_o) was plotted as a function of the inhibitor concentration (Fig. 5, middle panel). Fitting the data to the Michaelis-Menton equation for competitive inhibition revealed an initial inhibition constant of 1.79 nM for MT-DADMe-ImmA when tested against Bgp. Similar analysis of velocity data taken at 30–40 min into the assay demonstrates that the affinity of MT-DADMe-ImmA increases approximately ten-fold to 0.21 nM, consistent with the expected slow-onset inhibition reported for this compound against other bacterial MTNs (Fig. 5, bottom panel).[26,27,39,42,44,47]

A summary of the results shows that both the early transition state (MT-ImmA, HCY-ImmA, 5'-dEt-ImmA) and late transition state analogs (MT-DADMe-ImmA, BuT-DADMe-ImmA) bind with high affinity (K_i = 0.7–3nM) to all three borrelial enzymes (Table 3). All of these analogs also displayed slow-onset inhibition that resulted in a 3- to 27-fold increase in inhibitor affinity (K_i* = 0.05–0.8 nM). When the data for Bgp were examined across the five analogs, the late transition state analogs (0.21–0.33 nM) showed a modest improvement in affinity relative to the early transition state analogs (0.35–0.62 nM). MtnN was more susceptible to the early transition state inhibitors than Bgp and Pfs, but it also showed the highest affinity (0.05 nM) for the late transition state BuT-DADMe-ImmA analog. Late transition state analogs were consistently more potent against the cytoplasmic Pfs (0.06–0.2 nM) than the early transition state analogs (0.53–0.83 nM). While these inhibitors displayed affinities against *E. coli* and other bacterial MTNs that were generally 10- to 100-fold tighter than their subnanomolar affinities for the borrelial enzymes,[26,27,39,42,44,48], their tight binding properties suggest that saturating conditions should be achievable in culture and *in vivo*, which would be important for the inhibitors to achieve antibiotic activity.

3.4. MTN enzyme modeling.

Three-dimensional models of the borrelial MTNs were developed based on known crystal structures for the *E. coli*, *Vibrio*, and *Borrelia* MTNs.[26,27,39,49–52] Images of MT-DADMe-ImmA computationally docked into the modeled active sites for Bgp, MtnN, and Pfs are

Author Manuscript Author Manuscript Author Manuscript Author Manuscript

presented in Figure 6 to illustrate inhibitor-enzyme interactions important for the tight binding of the immucillin analogs. Amine groups on the purine form 3 or 4 hydrogen bonds with conserved aspartate residues (Bgp D189, D232; MtnN D195, D238; Pfs D160, D204) in the active site in all three enzymes. Hydrogen bond interactions were also found between the 2'-hydroxyl group and conserved glutamate residues in Bgp (E37) and Pfs (E11). Interestingly, in MtnN the most thermodynamically favorable docked structure of MT-DADMe-ImmA showed a small rotation in the active site such that the 3'-hydroxyl group hydrogen bonded to a conserved glutamate (E215) that is found in all three nucleosidases. Hydrophobic interactions in the active site are numerous (only a few are shown in the image). Several of the hydrophobic residues (Phe, Leu) that make up the 5'-alkylthio-binding pocket are supplied by the adjacent monomer of the homo-dimer (shown in green) and are completely conserved among the three enzymes. In general, the modeled images suggest that inhibitors that function well in one enzyme will probably exert similar effects across all three nucleosidases. This observation is supported by the enzyme inhibition data (Table 3).

3.5. MTN inhibitor cytotoxicity studies.

While compounds have been developed that have very potent inhibitory activity against MTNs from a variety of bacterial species, there are few reports of definitive antimicrobial activity by any of these MTN inhibitors. Early work exploring indazole-based inhibitors[53] and purine-based inhibitors[54] yielded compounds with nanomolar affinities for MTN, but generally produced minimum inhibitory concentrations (MICs) that were >20–30 μM (the highest concentrations tested). Treatment of *E. coli* or *V. cholera* cultures with MTN transition state analog inhibitors resulted in loss of MTN activity and interrupted autoinducer-2 synthesis and biofilm formation but did not appear to affect planktonic cell growth despite picomolar to femtomolar enzyme dissociation constants.[39] Recent reports on transition state analogs like BuT-DADMe-ImmA showed that they exhibited low picomolar inhibition constants for *Helicobacter* MTN and IC_{90} values for *in vitro Helicobacter* cultures that were as low as of 0.01 μg/mL.[42,48] Related studies of transition state analogs also demonstrated picomolar slow-onset inhibition of the *Campylobacter jejuni* MTN and *in vitro* inhibition of *Campylobacter* culture growth at low micromolar concentrations.[47] In each of these cases, the acute sensitivity of *Helicobacter* and *Campylobacter* to transition state analogs was proposed to result from interruption of the MTN-mediated hydrolysis of 6-amino-6-deoxyfutalosine, an early step in a novel futalosine biosynthetic pathway for menaquinone synthesis, which is required for electron transport in these organisms.[42,47,48,55,56] However, the menaquinone pathway is not evident in *Borrelia*, so the antibiotic activity we see with the immucillins is not due to this mechanism.

Other work on adenosine analogs and adenosine transition state analog inhibitors of purine nucleoside phosphorylases (PNPs) in protozoa have shown their antiparasitic activity and potential for targeting purine salvage in antibiotic development. For example, in *Plasmodium falciparum*, adenosine-based immucillin analogs like Immucillin-A (ImmA) inhibited parasite PNP at low picomolar concentrations, causing a "purine-less" cell death in malarial cultures with an IC_{50} of 35nM.[57,58] Similarly, in *Trichomonas vaginalis*, an ImmA transition state analog potently inhibited adenosine-preferring parasite PNP at low picomolar

Author Manuscript Author Manuscript Author Manuscript Author Manuscript

concentrations,[59] while the adenosine-based PNP inhibitor 2-fluoro-2'-deoxyadenosine inhibited cultured parasites with an IC_{50} of 106 nM.[60] These findings have bearing on the present work because, similar to *Plasmodium* and *Trichomonas*, *B. burgdorferi* is a purine auxotroph and its genome contains 70% A-T nucleotides.[12,22]

Overall, these findings support the idea that the antimicrobial effects of enzyme inhibitors on pathogen metabolism will depend on the underlying purine or methionine auxotrophy that makes salvage pathway activity critical for survival. However, these are not the only mechanisms to consider. The complete BSK-II medium used to culture *Borrelia* contains both methionine (94 μM) and purines in the form of 2'-deoxyadenosine and 2'-deoxyguanosine (36 μM each), which on the surface suggests that direct nutrient starvation by MTN inhibition could be by-passed. However, an examination of the *Borrelia* genome indicates that it lacks the gene for purine nucleoside phosphorylase (PNP, EC 2.4.2.1) that would produce the purine base from these nucleosides. Instead, these deoxynucleosides are converted to deoxyadenylate (dAMP) and deoxyguanylate (dGMP) by the action of deoxynucleoside kinase (EC 2.7.1.74), and onward to the corresponding deoxynucleotide triphosphates (dNTPs) for use in nucleic acid biosynthesis. The lack of PNP implicates MTN as the only enzyme in the cell that would produce adenine. This adenine has two cellular metabolic fates. First, adenine is the substrate for *Borrelia* adenine deaminase (EC 3.5.4.2) that generates hypoxanthine for use in inosine monophosphate (IMP) production and subsequent GTP synthesis. Second, adenine is converted by the action of *Borrelia* adenine phosphoribosyltransferase (APRTase, EC 2.4.2.7) into adenylate (AMP) and onward to ATP via the sequential actions adenylate kinase (EC 2.7.4.3) and nucleoside diphosphate kinase (EC 2.7.4.5). Ultimately this indicates a critical role for MTN in the initial steps of purine nucleotide metabolism, since *Borrelia* lacks the genes for the *de novo* synthesis of the purine moiety.

Other potential mechanisms to consider include the buildup of MTA, 5'dADO, and SAH, which may act as growth inhibitors in the cell through inhibition of polyamine synthesis, radical SAM reactions, and methylations, respectively.[21,61,62] However, the lack of obvious gene homologs of bacterial polyamine synthases and radical SAM enzymes suggest that these may not be applicable mechanisms in *Borrelia*. Homologs of DNA methyltransferases are present in the genome of *B. burgdorferi*[12,63], and these would produce SAH in the cell, but their susceptibility to SAH product inhibition, and the influence of this on cell survival remains a topic of future study to determine if this is a mechanism of action by which MTN inhibition exerts its effect.

We have previously reported on the antibiotic effect of four nucleoside-based MTN inhibitors of *B. burgdorferi* Bgp and Pfs, two of which showed MIC values less than 16 nM using a novel fluorescence based assay.[19] In the current study, we analyzed drug effects on the *B. burgdorferi* N40 strain (Fig. 7) using the commercially available reagent BacTiter-Glo™ (Promega), which reports cellular ATP content as a measure of microbial cell viability. After 24-hr exposure, both MT-DADMe-ImmA and BuT-DADMe-ImmA exerted similarly potent antibiotic effects, with IC_{50} values of 0.31μg/mL (106 nM) and 0.38μg/mL (113 nM), respectively. The late transition state analogs were substantively more effective than the ampicillin control, which demonstrated an IC_{50} of 1.07μg/mL (3.01 μM).

Author Manuscript Author Manuscript Author Manuscript Author Manuscript

In the context of purine salvage, all three MTNs likely play important roles in relieving the purine auxotropy found in *Borrelia*. By virtue of their cell surface/extracellular location, Bgp and MtnN could supply critical adenine from exogenous nucleosides, the uptake of which has been implicated in cell survival and infection of mammalian cells.[64,65] Interestingly, the IC_{50} values for the late transition state analogs are generally 3–4 orders of magnitude larger than their slow-onset inhibition constants, which suggests that inhibition of intracellular Pfs is ultimately the most important event for a cellular effect, since the membrane-bound/secreted Bgp and MtnN orthologs would be accessible to extracellular drug and therefore inhibited at lower concentrations. Similar large discrepancies between binding affinity and antibiotic effect have been hypothesized by other investigators to be due to poor drug permeability,[39] which may require higher concentrations of the nucleoside analogs to cross cellular membranes and reach the intracellular target (e.g. Pfs). However, other factors, including the intracellular concentration of the target enzyme may also explain this difference. For instance, if we estimate that the volume of the borrelial cell is ~ 1 μm^3 (or ~ 0.2 μm wide × 15 μm long), then a modest number of copies of the enzyme (e.g. 60) would equate to an intracellular MTN concentration of approximately 100 nM. This would suggest that while the transition state analogs exhibit sub-nanomolar affinities for the various MTNs, the higher concentrations of drug required to exert an antibiotic effect may be attributed to a stoichiometric requirement to have two molecules of tight binding inhibitor for every enzyme dimer present in the cell. Nevertheless, the precise mechanism by which MTN inhibition leads to *Borrelia* cell death remains a topic of future study.

In summary, *B. burgdorferi* is a purine auxotroph that expresses three MTN enzymes (Bgp, MtnN, Pfs) that play a primary role in the salvage of adenine. All three enzymes show activity for the native MTA, SAH, and 5'dADO substrates, producing adenine and the corresponding neutral sugar. Kinetic measurements indicate that Bgp and Pfs are the most active with enzyme efficiencies that reveal a preference for MTA, while the preferred substrate for MtnN is SAH. Transition state analogs showed potent slow-onset inhibition of all three enzymes with sub-nanomolar affinities. Importantly, the late stage transition state analogs, MT-DADMe-ImmA and BuT-DADMe-ImmA, demonstrated potent *in vitro* antibiotic activity with IC_{50} values of ~ 100 nM for *B. burgdorferi* cultures. Our initial assertion is that these compounds are exerting their antibiotic effect by interruption of critical adenine salvage, but future mechanistic studies will be required to validate this hypothesis. Overall, our results support further examination of *Borrelia* MTNs as antibiotic targets and the continued development of MTN inhibitors as antibiotics to treat Lyme borreliosis and other infections caused by organisms (e.g. *Campylobacter*, *Helicobacter*) that rely upon MTN activity for critical cellular functions and pathogenesis.

Acknowledgements

This work was supported by Institutional Development Awards (IDeA) from the National Institutes of Health under grants P20GM103408 (Idaho INBRE) and P20GM109095 (BSU COBRE in Matrix Biology) and NIH R01 AI089921 award to NP. JHT and KAC received added support from NIH grant R15GM125065. The authors also acknowledge the support from Idaho Beef Council development grants (to DX and KAC), the BSU Biomolecular Research Center with funding from the National Science Foundation grants #0619793 and #0923535, and the MJ Murdock Charitable Trust. The students MF, CG, ARH, RJK, and PE were the recipients of summer research fellowships from the Idaho INBRE program (P20GM103408), and NSF Louis Stokes Alliance for Minority Participation (to CG) under grant #0901996.

Author Manuscript Author Manuscript Author Manuscript Author Manuscript

References

1. Nelson CA, Saha S, Kugeler KJ et al. Incidence of clinician-diagnosed Lyme disease, United States, 2005–2010. Emerg Infect Dis 2015; 21: 1625–31. [PubMed: 26291194]
2. Clayton JL, Jones SG, Dunn JR et al. Enhancing Lyme disease surveillance by using administrative claims data, Tennessee, USA. Emerg Infect Dis 2015; 21: 1632–4. [PubMed: 26291336]
3. Kugeler KJ, Farley GM, Forrester JD et al. Geographic distribution and expansion of human Lyme disease, United States. Emerg Infect Dis 2015; 21: 1455–7. [PubMed: 26196670]
4. Wormser GP, Nadelman RB, Dattwyler RJ et al. Practice guidelines for the treatment of Lyme disease. The Infectious Diseases Society of America. Clin Infect Dis 2000; 31 Suppl 1: 1–14.
5. Wormser GP, Dattwyler RJ, Shapiro ED et al. The clinical assessment, treatment, and prevention of lyme disease, human granulocytic anaplasmosis, and babesiosis: clinical practice guidelines by the Infectious Diseases Society of America. Clin Infect Dis 2006; 43: 1089–134. [PubMed: 17029130]
6. Dersch R, Sommer H, Rauer S et al. Prevalence and spectrum of residual symptoms in Lyme neuroborreliosis after pharmacological treatment: a systematic review. J Neurol 2016; 263: 17–24. [PubMed: 26459093]
7. Embers ME, Hasenkampf NR, Jacobs MB et al. Variable manifestations, diverse seroreactivity and post-treatment persistence in non-human primates exposed to Borrelia burgdorferi by tick feeding. PLoS One 2017; 12: e0189071. [PubMed: 29236732]
8. Kaplan RF, Trevino RP, Johnson GM et al. Cognitive function in post-treatment Lyme disease: do additional antibiotics help? Neurology 2003; 60: 1916–22. [PubMed: 12821733]
9. Nemeth J, Bernasconi E, Heininger U et al. Update of the Swiss guidelines on post-treatment Lyme disease syndrome. Swiss Med Wkly 2016; 146: w14353.
10. Strle K, Stupica D, Drouin EE et al. Elevated levels of IL-23 in a subset of patients with post-lyme disease symptoms following erythema migrans. Clin Infect Dis 2014; 58: 372–80. [PubMed: 24218102]
11. Weitzner E, Visintainer P, Wormser GP. Comparison of males versus females with culture-confirmed early Lyme disease at presentation and at 11–20 years after diagnosis. Diagn Microbiol Infect Dis 2016; 85: 493–5. [PubMed: 27230991]
12. Fraser CM, Casjens S, Huang WM et al. Genomic sequence of a Lyme disease spirochaete, *Borrelia burgdorferi*. Nature 1997; 390: 580–6. [PubMed: 9403685]
13. Cluss RG, Silverman DA, Stafford TR. Extracellular secretion of the *Borrelia burgdorferi* Oms28 porin and Bgp, a glycosaminoglycan binding protein. Infect Immun 2004; 72: 6279–86. [PubMed: 15501754]
14. Fischer JR, LeBlanc KT, Leong JM. Fibronectin binding protein BBK32 of the Lyme disease spirochete promotes bacterial attachment to glycosaminoglycans. Infect Immun 2006; 74: 435–41. [PubMed: 16368999]
15. Parveen N, Leong JM. Identification of a candidate glycosaminoglycan-binding adhesin of the Lyme disease spirochete *Borrelia burgdorferi*. Mol Microbiol 2000; 35: 1220–34. [PubMed: 10712702]
16. Parveen N, Cornell KA, Bono JL et al. Bgp, a secreted glycosaminoglycan-binding protein of *Borrelia burgdorferi* strain N40, displays nucleosidase activity and is not essential for infection of immunodeficient mice. Infect Immun 2006; 74: 3016–20. [PubMed: 16622242]
17. Parveen N, Caimano M, Radolf JD et al. Adaptation of the Lyme disease spirochaete to the mammalian host environment results in enhanced glycosaminoglycan and host cell binding. Mol Microbiol 2003; 47: 1433–44. [PubMed: 12603746]
18. Cornell KA, Riscoe MK. Cloning and expression of *Escherichia coli* 5'-methylthioadenosine/S-adenosylhomocysteine nucleosidase: identification of the pfs gene product. Biochim Biophys Acta 1998; 1396: 8–14. [PubMed: 9524204]
19. Cornell KA, Primus S, Martinez JA et al. Assessment of methylthioadenosine/S-adenosylhomocysteine nucleosidases of *Borrelia burgdorferi* as targets for novel antimicrobials using a novel high-throughput method. J Antimicrob Chemother 2009; 63: 1163–72. [PubMed: 19376840]

Author Manuscript Author Manuscript Author Manuscript Author Manuscript

20. Riley SP, Bykowski T, Babb K et al. Genetic and physiological characterization of the *Borrelia burgdorferi* ORF BB0374-pfs-metK-luxS operon. Microbiology 2007; 153: 2304–11. [PubMed: 17600074]
21. Parveen N, Cornell KA. Methylthioadenosine/S-adenosylhomocysteine nucleosidase, a critical enzyme for bacterial metabolism. Mol Microbiol 2011; 79: 7–20. [PubMed: 21166890]
22. Pettersson J, Schrumpf ME, Raffel SJ et al. Purine salvage pathways among *Borrelia* species. Infect Immun 2007; 75: 3877–84. [PubMed: 17502392]
23. Schlachter S, Seshu J, Lin T, Norris S, Parveen N. The *Borrelia burgdorferi* glycosaminoglycan binding protein Bgp in the B31 strain is not essential for infectivity despite facilitating adherence and tissue colonization. Infect Immun 2018; 86: e00667–17. [PubMed: 29158428]
24. Sievers F, Wilm A, Dineen D et al. Fast, scalable generation of high-quality protein multiple sequence alignments using Clustal Omega. Mol Syst Biol 2011; 7: 539. [PubMed: 21988835]
25. Pace CN, Vajdos F, Fee L et al. How to measure and predict the molar absorption coefficient of a protein. Protein Sci 1995; 4: 2411–23. [PubMed: 8563639]
26. Singh V, Evans GB, Lenz DH et al. Femtomolar transition state analogue inhibitors of 5'-methylthioadenosine/S-adenosylhomocysteine nucleosidase from *Escherichia coli*. J Biol Chem 2005; 280: 18265–73. [PubMed: 15749708]
27. Singh V, Shi W, Almo SC et al. Structure and inhibition of a quorum sensing target from *Streptococcus pneumoniae*. Biochemistry 2006; 45: 12929–41. [PubMed: 17059210]
28. Rose PW, Prlic A, Bi C et al. The RCSB Protein Data Bank: views of structural biology for basic and applied research and education. Nucleic Acids Res 2015; 43: D345–56. [PubMed: 25428375]
29. Maestro. Schrödinger Release 2015–4: Maestro, Schrödinger, LLC, New York, NY 2015.
30. Prime. Schrödinger Release 2015–4: Prime, Schrödinger, LLC, New York, NY 2015.
31. Johnson M, Zaretskaya I, Raytselis Y et al. NCBI BLAST: a better web interface. Nucleic Acids Res 2008; 36: W5–9. [PubMed: 18440982]
32. Friesner RA, Banks JL, Murphy RB et al. Glide: a new approach for rapid, accurate docking and scoring. 1. Method and assessment of docking accuracy. J Med Chem 2004; 47: 1739–49. [PubMed: 15027865]
33. Glide. Schrödinger Release 2015–4: Glide, Schrödinger, LLC, New York, NY 2015.
34. The PyMOL Molecular Graphics System, Version 1.8; Schrödinger, LLC.
35. Pothineni VR, Wagh D, Babar MM et al. Identification of new drug candidates against Borrelia burgdorferi using high-throughput screening. Drug Des Devel Ther 2016; 10: 1307–22.
36. Lee JE, Luong W, Huang DJ et al. Mutational analysis of a nucleosidase involved in quorum-sensing autoinducer-2 biosynthesis. Biochemistry 2005; 44: 11049–57. [PubMed: 16101288]
37. Kamath VP, Zhang J, Morris PE Jr., et al. Synthesis of a potent 5'-methylthioadenosine/S-adenosylhomocysteine (MTAN) inhibitor. Bioorg Med Chem Lett 2006; 16: 2662–5. [PubMed: 16504506]
38. Evans GB, Furneaux RH, Greatrex B et al. Azetidine based transition state analogue inhibitors of N-ribosyl hydrolases and phosphorylases. J Med Chem 2008; 51: 948–56. [PubMed: 18251493]
39. Gutierrez JA, Crowder T, Rinaldo-Matthis A et al. Transition state analogs of 5'-methylthioadenosine nucleosidase disrupt quorum sensing. Nat Chem Biol 2009; 5: 251–7. [PubMed: 19270684]
40. Longshaw AI, Adanitsch F, Gutierrez JA et al. Design and synthesis of potent "sulfur-free" transition state analogue inhibitors of 5'-methylthioadenosine nucleosidase and 5'-methylthioadenosine phosphorylase. J Med Chem 2010; 53: 6730–46. [PubMed: 20718423]
41. Clinch K, Evans GB, Frohlich RF et al. Transition state analogue inhibitors of human methylthioadenosine phosphorylase and bacterial methylthioadenosine/S-adenosylhomocysteine nucleosidase incorporating acyclic ribooxocarbenium ion mimics. Bioorg Med Chem 2012; 20: 5181–7. [PubMed: 22854195]
42. Wang S, Haapalainen AM, Yan F et al. A picomolar transition state analogue inhibitor of MTAN as a specific antibiotic for *Helicobacter pylori*. Biochemistry 2012; 51: 6892–4. [PubMed: 22891633]

Author Manuscript Author Manuscript Author Manuscript Author Manuscript

43. Thomas K, Haapalainen AM, Burgos ES et al. Femtomolar inhibitors bind to 5'-methylthioadenosine nucleosidases with favorable enthalpy and entropy. Biochemistry 2012; 51: 7541–50. [PubMed: 22931458]
44. Haapalainen AM, Thomas K, Tyler PC et al. *Salmonella enterica* MTAN at 1.36 A resolution: a structure-based design of tailored transition state analogs. Structure 2013; 21: 963–74. [PubMed: 23685211]
45. Namanja-Magliano HA, Stratton CF, Schramm VL. Transition state structure and inhibition of Rv0091, a 5'-deoxyadenosine/5'-methylthioadenosine nucleosidase from Mycobacterium tuberculosis. ACS Chem Biol 2016; 11: 1669–76. [PubMed: 27019223]
46. Namanja-Magliano HA, Evans GB, Harijan RK et al. Transition state analogue inhibitors of 5'-deoxyadenosine/5'-methylthioadenosine nucleosidase from Mycobacterium tuberculosis. Biochemistry 2017; 56: 5090–8. [PubMed: 28836767]
47. Ducati RG, Harijan RK, Cameron SA et al. Transition-state analogues of *Campylobacter jejuni* 5'-methylthioadenosine nucleosidase. ACS Chem Biol 2018; 13: 3173–83. [PubMed: 30339406]
48. Wang S, Cameron SA, Clinch K et al. New antibiotic candidates against *Helicobacter pylori*. J Am Chem Soc 2015; 137: 14275–80. [PubMed: 26494017]
49. Lee JE, Cornell KA, Riscoe MK et al. Structure of *E. coli* 5'-methylthioadenosine/S-adenosylhomocysteine nucleosidase reveals similarity to the purine nucleoside phosphorylases. Structure 2001; 9: 941–53. [PubMed: 11591349]
50. Lee JE, Cornell KA, Riscoe MK et al. Structure of *Escherichia coli* 5'-methylthioadenosine/S-adenosylhomocysteine nucleosidase inhibitor complexes provide insight into the conformational changes required for substrate binding and catalysis. J Biol Chem 2003; 278: 8761–70. [PubMed: 12496243]
51. Lee JE, Settembre EC, Cornell KA et al. Structural comparison of MTA phosphorylase and MTA/AdoHcy nucleosidase explains substrate preferences and identifies regions exploitable for inhibitor design. Biochemistry 2004; 43: 5159–69. [PubMed: 15122881]
52. Lee JE, Singh V, Evans GB et al. Structural rationale for the affinity of pico- and femtomolar transition state analogues of *Escherichia coli* 5'-methylthioadenosine/S-adenosylhomocysteine nucleosidase. J Biol Chem 2005; 280: 18274–82. [PubMed: 15746096]
53. Li X, Chu S, Feher VA et al. Structure-based design, synthesis, and antimicrobial activity of indazole-derived SAH/MTA nucleosidase inhibitors. J Med Chem 2003; 46: 5663–73. [PubMed: 14667220]
54. Tedder ME, Nie Z, Margosiak S et al. Structure-based design, synthesis, and antimicrobial activity of purine derived SAH/MTA nucleosidase inhibitors. Bioorg Med Chem Lett 2004; 14: 3165–8. [PubMed: 15149667]
55. Li X, Apel D, Gaynor EC et al. 5'-methylthioadenosine nucleosidase is implicated in playing a key role in a modified futalosine pathway for menaquinone biosynthesis in *Campylobacter jejuni*. J Biol Chem 2011; 286: 19392–8. [PubMed: 21489995]
56. Kim RQ, Offen WA, Davies GJ et al. Structural enzymology of *Helicobacter pylori* methylthioadenosine nucleosidase in the futalosine pathway. Acta Crystallogr D Biol Crystallogr 2014; 70: 177–85. [PubMed: 24419390]
57. Kicska GA, Tyler PC, Evans GB et al. Purine-less death in *Plasmodium falciparum* induced by immucillin-H, a transition state analogue of purine nucleoside phosphorylase. J Biol Chem 2002; 277: 3226–31. [PubMed: 11706018]
58. Evans GB, Tyler PC, Schramm VL. Immucillins in infectious diseases. ACS Infect Dis 2018; 4: 107–17. [PubMed: 29151351]
59. Rinaldo-Matthis A, Wing C, Ghanem M et al. Inhibition and structure of *Trichomonas vaginalis* purine nucleoside phosphorylase with picomolar transition state analogues. Biochemistry 2007; 46: 659–68. [PubMed: 17223688]
60. Zang Y, Wang WH, Wu SW et al. Identification of a subversive substrate of *Trichomonas vaginalis* purine nucleoside phosphorylase and the crystal structure of the enzyme-substrate complex. J Biol Chem 2005; 280: 22318–25. [PubMed: 15817485]

Author Manuscript Author Manuscript Author Manuscript Author Manuscript

61. Hiscox MJ, Driesener RC, Roach PL. Enzyme catalyzed formation of radicals from S-adenosylmethionine and inhibition of enzyme activity by the cleavage products. Biochim Biophys Acta 2012; 1824:1165–77. [PubMed: 22504666]
62. Hendricks CL, Ross JR, Pichersky E, Noel JP, Zhou ZS. An enzyme-coupled colorimetric assay for S-adenosylmethionine-dependent methyltransferases. Anal Biochem 2004; 326: 100–5. [PubMed: 14769341]
63. Hughes CA, Johnson RC. Methylated DNA in *Borrelia* species. J Bacteriol 1990; 172: 6602–4. [PubMed: 2228977]
64. Jain S, Sutchu S, Rosa PA et al. *Borrelia burgdorferi* harbors a transport system essential for purine salvage and mammalian infection. Infect Immun 2012; 80: 3086–93. [PubMed: 22710875]
65. Jain S, Showman AC, Jewett MW. Molecular dissection of a *Borrelia burgdorferi in vivo* essential purine transport system. Infect Immun 2015; 83: 2224–33. [PubMed: 25776752]

Author Manuscript Author Manuscript Author Manuscript Author Manuscript

Highlights

- *Borrelia burgdorferi* uniquely possesses secreted, membrane-bound, and intracellular MTA/SAH nucleosidases (MTNs)
- Enzyme analysis indicates both unique properties and shared activities for the three enzymes
- Nucleoside transition state analogs exhibit potent inhibitor activity against all three enzymes and inhibit in vitro borrelial growth
- Borrelial MTNs appear to be good targets for the development of antibiotics to treat Lyme disease

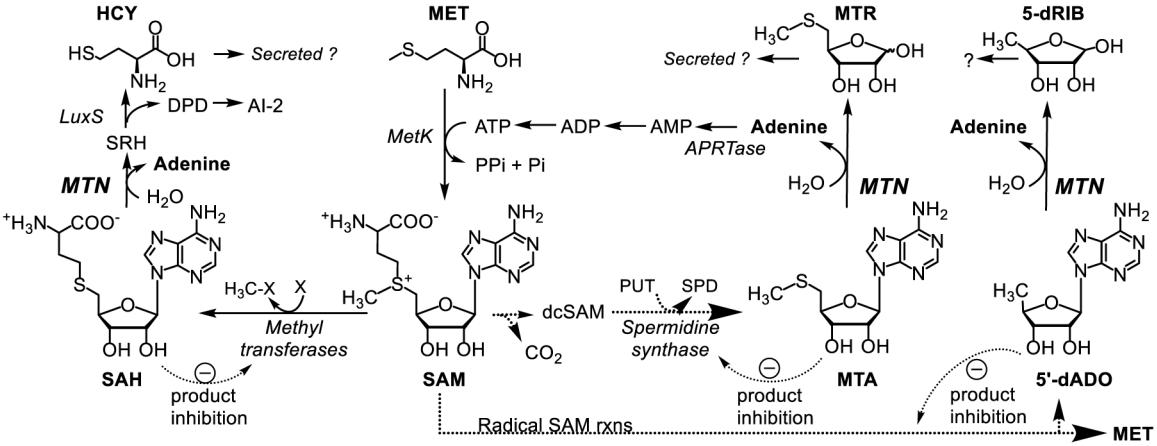

Figure 1. S-adenosylmethionine (SAM, AdoMet)-dependent metabolic pathways.

MTA/SAH nucleosidase (MTN or MTAN, EC) is responsible for catabolic hydrolysis of 5'-methylthioadenosine (MTA), S-adenosylhomocysteine (SAH, AdoHcy), and 5'-deoxyadenosine (5'dADO) to adenine and the corresponding sugar: methylthioribose (MTR), S-ribosylhomocysteine (SRH), and 5-deoxyribose (5-dRIB), respectively. Biological methylations generate SAH. Enzymatic decarboxylation of SAM yields dcSAM, which serves as the propylamine donor with putrecine (PUT) to generate spermidine (SPD) and MTA. Methionine (MET) and 5'dADO are the byproducts of radical SAM reactions. These latter two paths are represented by dashed lines, since the enzymes do not appear to be present in *Borrelia* but are common in many other bacteria. The enzyme S-ribosylhomocysteine lyase (LuxS, EC 4.4.1.21) converts SRH to homocysteine (HCY) and dihydroxypentanedione (DPD), which spontaneously forms the quorum sensing molecule autoinducer-2 (AI-2). Adenine re-enters the nucleotide pools by the action of adenine phosphoribosyl transferase (APRTase, EC 2.4.2.7). SAM synthetase (MetK, EC 2.5.1.6) uses ATP and MET to regenerate SAM. *B. burgdorferi* lacks the enzymes responsible for salvaging HCY and MTR back to methionine, and the fate of 5-deoxyribose (5-dRIB) is unknown in this organism.

Author Manuscript Author Manuscript Author Manuscript Author Manuscript

Author Manuscript Author Manuscript Author Manuscript Author Manuscript

```
EC Pfs   1                                   MK
Bgp      1           MNNCLIKFFIFLLVFSNSYVAFSKNVN
MtnN     1 MKIKNIANILIFFLSIVLNSWGNESKINTPNENSQSN
Pfs      1                                    M

EC Pfs   3 IGIIGAMEEEVTLLRDKIENRQTISLGGC----EIYT
Bgp     28 VLIVTAMDSEFDQINKLMSNKEEIVLKEYGLNKKILK
MtnN    38 ILIISATKAEIEEINKIIQNKKYISIEEHRRKKKIAI
Pfs      2 ILIISAMQEESEEINKILDNKEEIVLNDYLENKKIYK
           + *+ *   *   +   + *+  * +        *

EC Pfs  36 GQLNGTEVALLKSGIGKVAAALGATLLLEHCKPDVII
Bgp     65 GKLSNRNVMVIICGVGKVNAGVWTSYILSKYNISHVI
MtnN    75 GKLMDHNIITIATGVGKINTALWTSYIISKYKISHII
Pfs     39 GKILGKDVISLTTGIGKVNAATWSSQIISKYKITHII
           *++    +  + +*+**+ +   ++ ++ +     +*

EC Pfs  73 NTGSAGGLAPT----LKVGDIVVSDEARYHDADVTAF
Bgp    102 NSGVAGGVVSAKYKDIKVGDVVVSSEVAYHDVDLTKF
MtnN   112 NAGVASGIYSDKNKFIKIGDVVISTETTSYDFDLHRF
Pfs     76 NSGSSGGIKENSN--LKILDIIVSSETAYYDFDLTKF
           *+* + *+       +*+ *+++* *    * *+  *

EC Pfs 106 GYEYGQLP-GCPAGFKADDKLIAAAEACIAE--LNLN
Bgp    139 GYKVGQLTGGLPQKFNANKNLIKNAIEAIKSKVGGSN
MtnN   149 GYEIGHVP-EHPKKFKANTALIRKTSKIKIN---NIT
Pfs    111 GHKIGQVP-NLPQKFKADEELLKKVANIVDNKLLNID
           *   *++    *  * *   *+            +

EC Pfs 140 AVRGLIVSGDAFINGSVGLAKIRHNFPQAIAVEMEAT
Bgp    176 AYSGLIVSGDQFIDPTY-INKIIGNFKDVIAVEMEGA
MtnN   182 SYMGLIITGDQFIDHQT-FQEIPEEFENAIAIDMESA
Pfs    147 IHIGLILTGDQFVDNEKNLETIKKNFKDALAVDMEGA
              ***++** *+        *   *   +*++** +

EC Pfs 176 AIAHVCHNFNVPFVVVRAISDVADQQ-SHLSFDEFLA
Bgp    212 AIGHVSHMFNIPFIVIRSISDIVNKEGNEVEYSKFSK
MtnN   218 AMAQVAYGFKIPFIIIRGISDIVNNENNYDDYKKFLK
Pfs    184 AIAQVAHIFKIPFIIIRSISDLPNNKDNHIDFNKFLK
           *+ +*+  * +**+++* ***+         +  *

EC Pfs 211 VAAKQSSLMVESLVQKLAHG              230
Bgp    249 IAAFNSAKVVQEILRKL                 265
MtnN   255 KASSSSAKIVENLIKLM                 271
Pfs    221 TSSINSSKMTKELIRLI                 237
           ++  *+ +   +++ +
```

Figure 2. Clustal Omega multiple amino acid sequence alignment of MTNs.

The sequence of the cytoplasmic *E. coli* MTN (EC Pfs) is compared to *Borrelia burgdorferi* surface (Bgp), surface/periplasmic/secreted (MtnN), and cytoplasmic (Pfs) MTNs. The amino terminal signal sequences for Bgp and MtnN are underlined. Conserved essential catalytic aspartate and glutamate residues are bolded and underlined. An asterisk marks identical amino acids, while a “+” indicates conserved amino acids in all four sequences.

Author Manuscript Author Manuscript Author Manuscript Author Manuscript

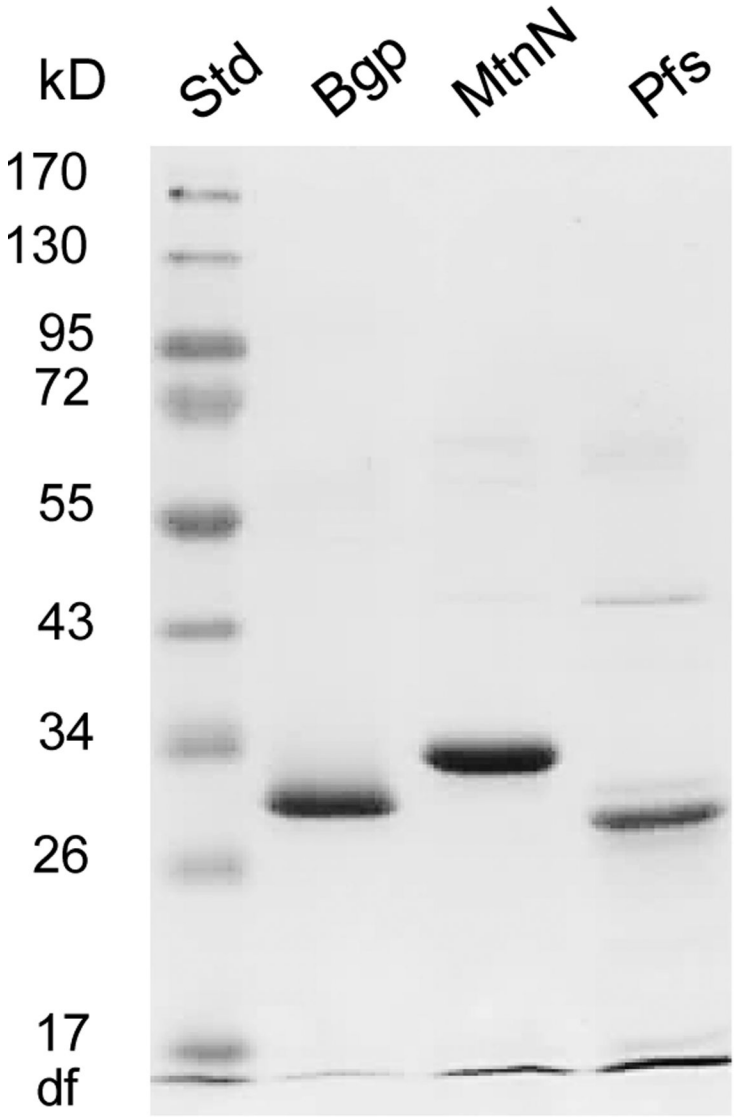

Figure 3. SDS-PAGE of purified recombinant *B. burgdorferi* MTNs.

Recombinant enzymes were purified using Co^{2+} affinity chromatography, electrophoresed on a 15% SDS-polyacrylamide gel, and stained with Coomassie blue. All three enzymes showed apparent molecular weights of 28–32 kD consistent with predicted monomeric molecular weights of the enzymes containing the recombinant hexahistidine tag.

Author Manuscript Author Manuscript Author Manuscript Author Manuscript

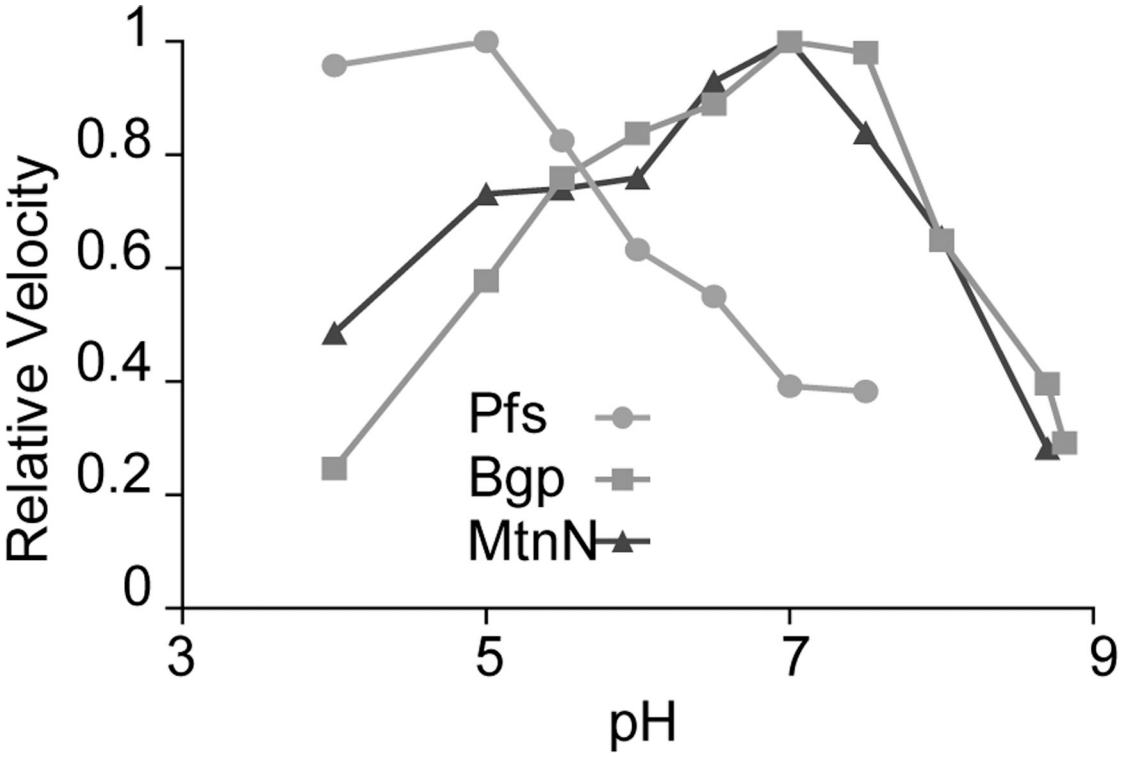

Figure 4. Influence of pH on enzyme activity for the three *B. burgdorferi* MTNs.

Bgp and MtnN are optimally active at pH 7, while Pfs functions preferentially under more acidic conditions (pH 5).

Author Manuscript Author Manuscript Author Manuscript Author Manuscript

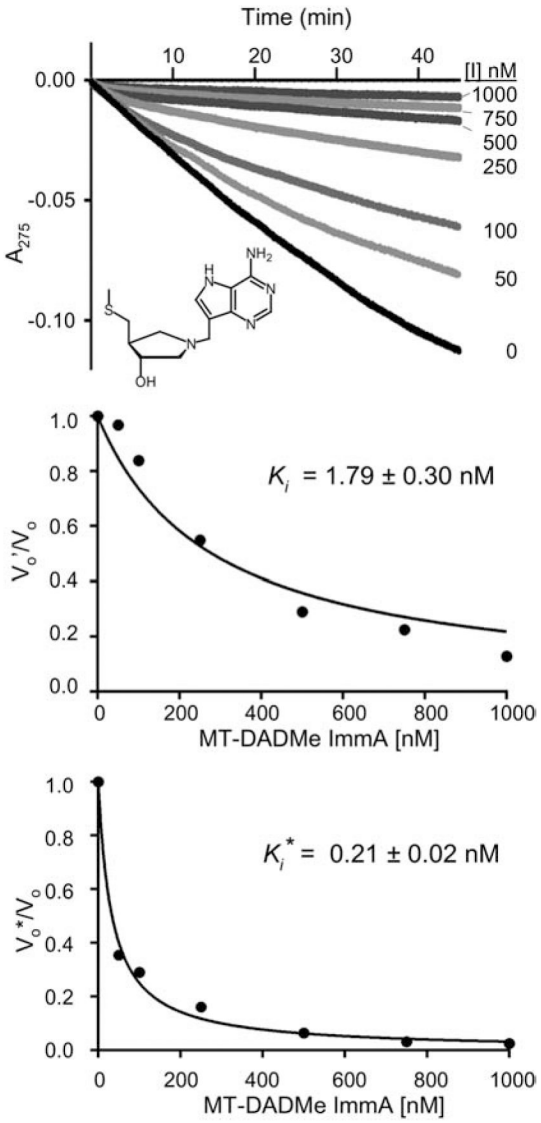

Figure 5. Inhibition of *B. burgdorferi* Bgp by MT-DADMe-ImmA.

Enzyme activity was assayed using a direct measurement of substrate conversion to product that corresponds to a decrease in absorbance at 275 nm (top panel). The concentration of inhibitor (nM) used for each trace is indicated at the right. Slopes of the data (0–5 min, top panel) were used to create a ratio of initial velocities and calculate the early onset inhibition constant (K_i) (middle panel). Later slopes (30–40 min) were used to calculate the delayed onset inhibition constant (K_i^*) (bottom panel).

Author Manuscript Author Manuscript Author Manuscript Author Manuscript

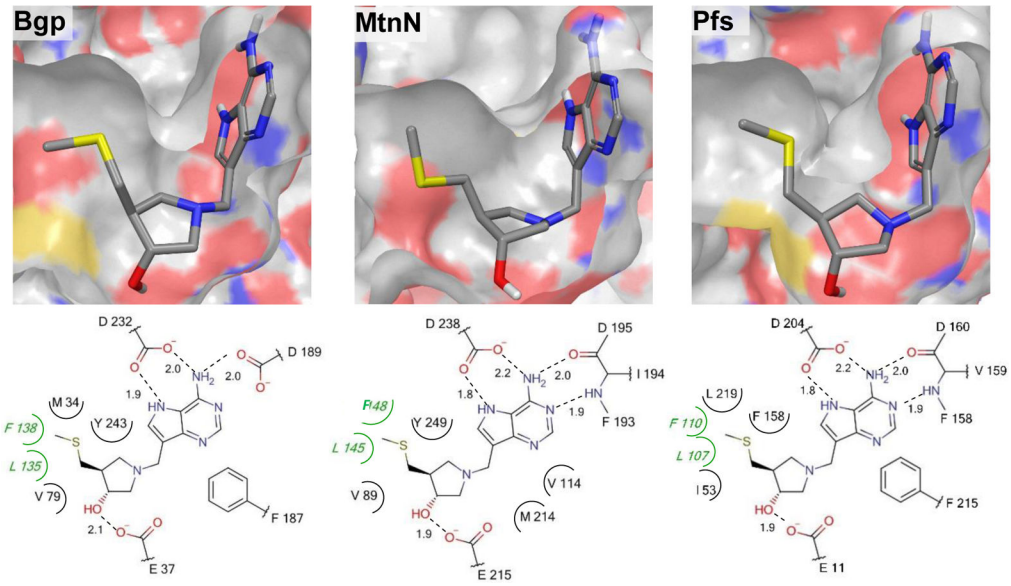

Figure 6. Docked structures of MT-DADMe ImmA in the enzyme active sites of Bgp, MtnN, and Pfs.

The top panels show the surface electrostatic charges in the active site (electronegative in red, electropositive in blue, sulfur in yellow). The molecular bond interactions between the drug and active site amino acids are depicted in the lower panels. H-bonds between the nucleoside analog and catalytically critical aspartate and glutamate residues are indicated by dashed lines, and hydrophobic interactions are indicated by arcs. Residues in green indicate amino acid contributions to the 5'-alkylthio binding pocket that are supplied by the partner monomer in the homo-dimeric enzyme.

Author Manuscript Author Manuscript Author Manuscript Author Manuscript

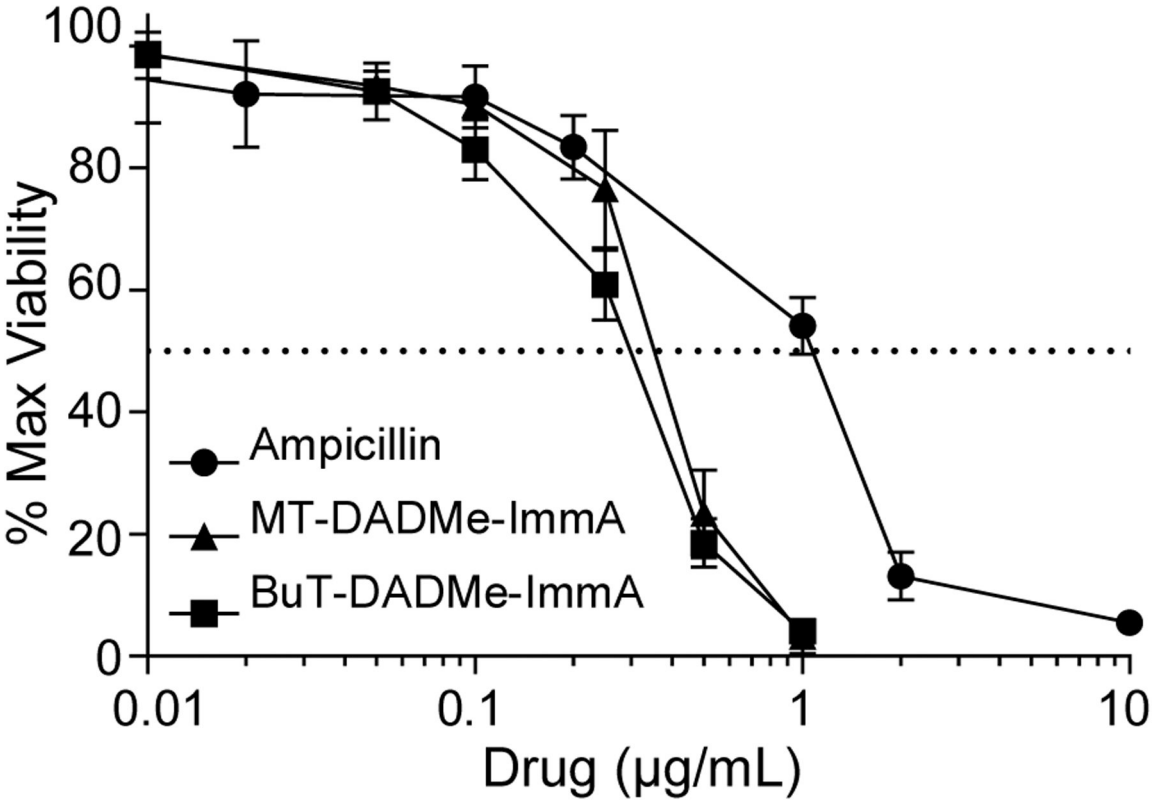

Figure 7. Antimicrobial activity of MTN inhibitors against *B. burgdorferi* strain N40.

Cell viability was measured using a BacTiter-Glo bioluminescent assay after 24 h exposure to drug. The graph represents the mean percentage of drug-free control of two independent experiments with individual drug concentrations tested in triplicate. Standard error bars are shown. The IC_{50} values for MT-DADMe-ImmA (0.31 μg/mL) and BuT-DADMe-ImmA (0.38 μg/mL) were less than the ampicillin control (1.07 μg/mL).

Author Manuscript Author Manuscript Author Manuscript Author Manuscript

Table 1.

Summary of *Borrelia* MTN kinetic parameters*

Enzyme	Substrate	K_m (μM)	k_{cat} (min^{-1})	k_{cat}/Km ($min^{-1}\mu M^{-1}$)
Bgp	MTA	0.49 ± 0.01	111 ± 20	228 ± 44
	SAH	1.96 ± 0.67	105 ± 12	53 ± 8
	5'dADO	1.79 ± 0.52	92 ± 28	51 ± 16
MtnN	MTA	9.09 ± 1.62	93 ± 5	10 ± 1
	SAH	2.04 ± 0.44	33 ± 1	16 ± 3
	5'dADO	10.46 ± 0.75	44 ± 1	4 ± 0.3
Pfs	MTA	0.61 ± 0.16	107 ± 3	175 ± 19
	SAH	0.75 ± 0.16	94 ± 5	144 ± 31
	5'dADO	1.37 ± 0.37	162 ± 9	118 ± 24

*Results expressed as the mean ± standard error of the mean (SEM)

Author Manuscript Author Manuscript Author Manuscript Author Manuscript

Table 2.

Borrelia MTN specific activities (U/mg) for native and alternate substrates*

	Enzyme					
Substrate	**Bgp**		**MtnN**		**Pfs**	
5'-methylthioadenosine (MTA)	6.89 ± 0.02	(100)	4.20 ± 0.10	(100)	6.33 ± 0.36	(100)
S-adenosylhomocysteine (SAH)	6.43 ± 0.43	(93)	3.50 ± 0.14	(83)	5.55 ± 0.12	(88)
5'-deoxyadenosine (5'-dADO)	5.10 ± 0.16	(74)	2.30 ± 0.15	(55)	5.20 ± 0.05	(82)
5'-ethylthioadenosine (ETA)	5.56 ± 0.12	(80)	3.65 ± 0.35	(87)	2.31 ± 0.17	(37)
5'-propylthioadenosine (PTA)	3.96 ± 0.05	(57)	2.51 ± 0.12	(60)	2.21 ± 0.07	(35)
5'-isopropylthioadenosine (iPTA)	4.55 ± 0.32	(66)	1.77 ± 0.08	(42)	2.47 ± 0.04	(39)
5'-butylthioadenosine (BTA)	2.25 ± 0.09	(33)	0.49 ± 0.02	(12)	1.78 ± 0.08	(28)
adenosine (ADO)	1.76 ± 0.05	(26)	0.36 ± 0.02	(9)	0.32 ± 0.04	(5)
5'-chloroadenosine (C1ADO)	1.17 ± 0.03	(17)	0.34 ± 0.01	(8)	0.82 ± 0.07	(13)
adenosine monophosphate (AMP)	0.05 ± 0.01	(1)	0.13 ± 0.01	(3)	0.12 ± 0.03	(2)

*Results expressed are the mean specific activity ± SEM. Values in parentheses represent the percent of maximum activity. 1U = 1 μmol/min MTA hydrolyzed to adenine and 5-methylthioribose.

Author Manuscript Author Manuscript Author Manuscript Author Manuscript

Table 3.

Summary of transition state analog enzyme inhibition constants (nM)*

Early Transition State Analog

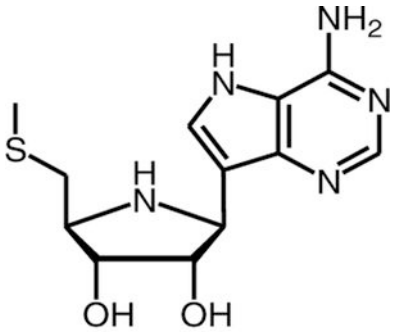

MT-ImmA

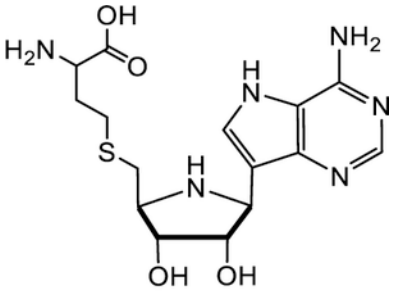

HCY-ImmA

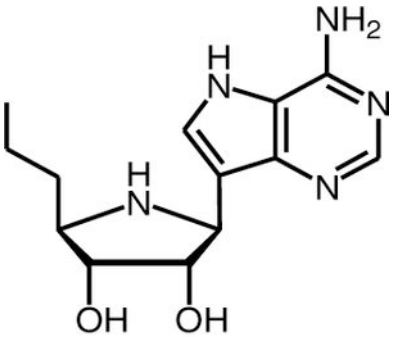

5' dEt-ImmA

	K_i	K_i*	K_i	K_i*	K_i	K_i*
Bgp	2.71±0.34	0.62±0.12	1.87±0.32	0.56±0.07	2.48±0.38	0.35±0.02
MtnN	0.88±0.12	0.11±0.02	ND	ND	1.48=0.17	0.58±0.05
Pfs	3.07±0.27	0.74±0.11	9.46±2.64	0.83±0.30	10.49±2.01	0.53±0.15

Late Transition State Analogs

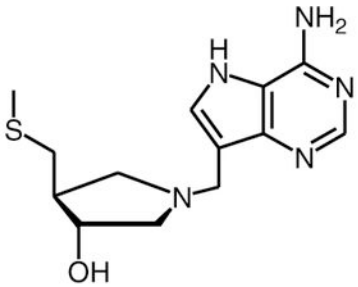

MT-DADMe-ImmA

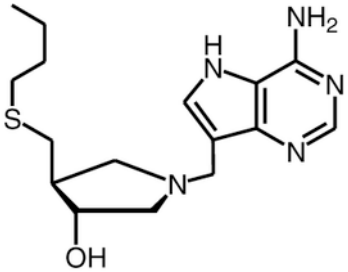

BuT-DADMe-ImmA

	K_i	K_i*	K_i	K_i*
Bgp	1.79±0.30	0.21±0.02	1.27±0.33	0.33±0.15
MtnN	2.93±0.42	0.63±0.09	1.38±0.12	0.05±0.01
Pfs	0.73±0.41	0.06±0.01	1.96±0.28	0.20±0.04

*Inhibition constants reported as the mean concentration in nM ± SEM.

K_i = early onset inhibition, K_i* = delayed onset inhibition, ND = not determined.